

EMERGENT SPECTRA FROM DISKS SURROUNDING KERR BLACK HOLES: EFFECT OF PHOTON TRAPPING AND DISK SELF-SHADOWING

CENTER FOR ASTROPHYSICS, DEPARTMENT OF ASTRONOMY, UNIVERSITY OF SCIENCES AND TECHNOLOGY OF CHINA, HEFEI
230026, CHINA

Draft version November 21, 2018

ABSTRACT

Based on a new estimation of their thickness, the global properties of relativistic slim accretion disks are investigated in this work. The resulting emergent spectra are calculated using the relativistic ray-tracing method, in which we neglect the self-irradiation of the accretion disk. The angular dependence of the disk luminosity, the effects of the heat advection and the disk thickness on the estimation of the black hole spin are discussed. Compare to the previous works, our improvements are that we use the self-consistent disk equations and we consider the disk self-shadowing effect. We find that at the moderate accretion rate, the radiation trapped in the outer region of the accretion disks will escape in the inner region of the accretion disk and contribute to the emergent spectra. At the high accretion rate, for the large inclination and large black hole spin, both the disk thickness and the heat advection have significant influence on the emergent spectra. Consequently, these effects will influence the measurement of the black hole spin based on the spectra fitting and influence the angular dependence of the luminosity. For the disks around Kerr black holes with $a = 0.98$, if the disk inclination is greater than 60° , and their luminosity is beyond 0.2 Eddington luminosity, the spectral model which is based on the relativistic standard accretion disk is no longer applicable for the spectra fitting. We also confirm that the effect of the self-shadowing is significantly enhanced by the light-bending, which implies that the non-relativistic treatment of the self-shadowing is inaccurate. According to our results, the observed luminosity dependence of the measured spin suggests that the disk self-shadowing significantly shapes the spectra of GRS 1915+105, which might lead to the underestimation of the black hole spin for the high luminosity states.

Subject headings: accretion, accretion disks - binaries: close - black hole physics - X-rays: stars

1. INTRODUCTION

The standard accretion disk model (SSD, Shakura & Sunyaev 1973) and its relativistic generalization (Novikov & Thorne 1973) are widely used in modeling the spectral energy distribution (SED) of both active galactic nuclei (AGNs) and the galactic black hole binaries. Recently, based on the relativistic SSD, the spins of the black holes in several galactic black hole binaries are measured by fittings of their SED (Li et al. 2005; Shafee et al. 2006; McClintock et al. 2006; Middleton et al. 2006). One major advantage of standard accretion disk model is its simplicity, i.e., it assumes that the fluid undergoes the Keplerian motion and the energy generated by the viscous heating is radiated locally. Besides, in this model, the disk terminates at the Innermost Stable Circular Orbit (ISCO), and the matter inside ISCO is cold.

However, when the accretion rate is relatively high ($\dot{M} > 0.1\dot{M}_{\text{edd}}$), in the inner region of the accretion disks, several effects will make these assumptions invalid. One such effect is the heat advection. When the vertical diffusion time scale is larger than the accretion time scale, substantial amount of heat is trapped inside the accretion flow and not able to escape to the infinity (Begelman 1978; Begelman & Meier 1982). This will make the local flux different from that from the SSD model and affect the profile of the radial temperature. Also, the advected heat will provide an additional pressure, which makes the disk rotation no longer Keplerian. Besides, because the heat trapped inside the accretion flow, the region inside ISCO is not cold any more.

The self-consistent treatment of these effects needs to model the energy and momentum balance in the disk, one widely used method is based on the radiative MHD simulation. Although the numerical simulations have the advantage of treating the physical effects self-consistently, the huge amount of computation makes it difficult to give the qualitative fitting of the observational data. One complementary approach is to solve the energy and momentum equations of the accretion flow in terms of the ordinary differential equations (ODEs). Compared to the simulations, this method can effectively take into account the dynamical effects, while maintaining its conciseness. In this work, we use the ODE form disk equations (Paczynski & Bisnovaty-Kogan 1981; Abramowicz et al. 1988; Chen & Taam 1993; Peitz & Appl 1997; Gammie & Popham 1998), and explore the solutions at both the medium and high accretion rate (where the disk is call the “slim disk”; Abramowicz et al. 1988). We use the relativistic disk equations in our work (Abramowicz et al. 1996; Beloborodov 1998; Shimura & Manmoto 2003) to investigate the effects of the black hole spin.

The physical properties of the black hole and the accretion disks are deduced mainly from their observed SED. It is well known that the structure and the SED of the slim disk differ significantly from that of SSD (Wang & Zhou 1999; Wang et al. 1999). The disk SED is influenced by a handful of effects, such as the Doppler effect, the relativistic beaming, the gravitational redshift, the gravitational -bending, and the disk self-shadowing. As the accretion rate increases, the disk becomes geometrically thick, and the disk self-shadowing (Wu & Wang 2007) becomes significant. In this work, we employ a ray-tracing approach (e.g. Fanton et al. 1997; Cadez et al. 1998) to explore the final spectra at the different viewing angles.

³ Key Laboratory for Research in Galaxies and Cosmology, Shanghai Astronomical Observatory, Chinese Academy of Sciences, Shanghai 200030, China; cxw@shao.ac.cn

Due to their disk-like geometry, the radiation from the accretion disks is far from the isotropy, and the emergent luminosity is thus angular dependent (e.g. Heinzler et al. 2006). For a slab of optically thick material without velocity, the disk luminosity simply varies as $L \sim \cos \theta$ in the flat spacetime. In fact, because of its thickness and rotation, the angular dependence of the disk luminosity is expected to be different from that of the simple slab, further analysis is thus needed. In this paper, we calculate the angular dependence of the disk luminosity under different inclinations and the black hole spin.

The spin of GRS 1915+105 is debated in the literature (McClintock et al. 2006; Middleton et al. 2006). By fitting the disk blackbody component, McClintock et al. (2006) found that the spin is near extreme, while Middleton et al. (2006) found the spin is moderate, with $a \sim 0.8$. To show how the spin determination is influenced by the heat advection and disk self-shadowing, we re-simulate the observation carried out by McClintock et al. (2006) with our model and confirm the luminosity dependence of the measured spin as found by McClintock et al. (2006).

In this work, the black hole mass in our canonical model is taken to be $10M_{\odot}$. However, due to the physical similarities between the accretion disks around the stellar-mass black holes and those around the supermassive black holes, our results can be easily generalized to the supermassive black holes and predict the SED of AGNs under the simple scaling.

This paper organized as follows. In section 2, we describe briefly our disk model and the ray-tracing method. In Section 3.1–Section 3.3, we present our numerical results of the global disk structure. In Section 4, we present our results on the SED of the disk, focusing on the differences between the SED of the dynamical disk model and that of the SSD. The angular dependence of the total luminosity is given in Section 5. In Section 6, implications for estimating the black hole spin are discussed. In Section 7, various observational implications of the disk self-shadowing as well as the spin of GRS 1915+105 are discussed. Finally, in Section 8 we summarize our conclusions.

2. THE RELATIVISTIC SLIM MODEL

2.1. The Dynamical Disk Model

The basic equations governing the disk structure used in our work are similar to those given in Shimura & Manmoto (2003). In the Boyer–Lindquist coordinates, expanding around the equatorial plane up to $(z/r)^0$ terms, the metric takes the form (Novikov & Thorne 1973, the geometric unit $G = C = M = 1$ is taken):

$$ds^2 = -r^2 \frac{\Delta}{A} dt^2 + \frac{A}{r^2} (d\phi - \omega dt)^2 + \frac{r^2}{\Delta} dr^2 + dz^2, \quad (1)$$

with

$$\begin{aligned} \Delta &= r^2 - 2r + a^2, \\ A &= r^4 + r^2 a^2 + 2ra^2, \\ \omega &= \frac{2ar}{A}, \end{aligned}$$

where a is the dimensionless spin of the black hole.

The mass conservation takes form

$$\dot{M} = 2\pi \Delta^{1/2} \Sigma \gamma_r V, \quad (2)$$

where \dot{M} is the mass accretion rate, and W and Σ are integrated pressure and density, defined as $W = \int p dz$, $\Sigma =$

$\int \rho dz$. Here, p means pressure and ρ means density, the subscript “0” denotes the corresponding value at the equatorial plane, and H is the scale height of the accretion disk. γ_r is the radial Lorentz factor of the fluid.

The angular momentum conservation reads

$$\frac{\dot{M}}{2\pi} (L - L_{\text{in}}) = \alpha \frac{A^{3/2} \Delta^{1/2} \gamma_{\phi}^3}{r^5} W, \quad (3)$$

where L is the specific angular momentum, L_{in} is the specific angular momentum at the inner boundary of the accretion flow, and γ_{ϕ} is the Lorentz factor in the ϕ direction as defined in Manmoto (2000). As the viscosity prescription used here is conventional (Narayan 1992), at the inner part of the accretion disk, our result may be inaccurate in principle. However, the causal viscosity is still somewhat putative and differs from the conventional one only close to or inside the ISCO. Thus, the disk spectrum in our Kerr case is robust in the sense that the sonic point is very close to the event horizon of the black hole, while the disk spectrum in the Schwarzschild case may be shifted a bit due to the different treatment of the prescription of the viscosity.

The momentum equation and energy equation take the forms as follows:

Momentum equation:

$$\gamma_r^2 V \frac{dV}{dr} = -\frac{1}{\Sigma} \frac{dW}{dr} - \frac{\gamma_{\phi}^2 A}{r^4 \Delta} \frac{(\Omega - \Omega_{\text{k}}^+)(\Omega - \Omega_{\text{k}}^-)}{\Omega_{\text{k}}^+ \Omega_{\text{k}}^-}, \quad (4)$$

where

$$\Omega_{\text{k}}^{\pm} = \pm \frac{1}{r^{\frac{3}{2}} \pm a}$$

is the Keplerian angular velocity of the direct (“+ sign”) and retrograde (“-” sign) circular orbit, respectively. And here

$$\gamma_{\phi} = \left(1 + \frac{r^2 L^2}{\gamma_r^2 A}\right)^{1/2}$$

is Lorentz factor of v_{ϕ} ,

$$\Omega = \omega + \tilde{\Omega} = \omega + \frac{r^3 \Delta^{1/2} L}{A^{3/2} \gamma_r \gamma_{\phi}}.$$

Energy equation:

$$Q_{\text{vis}}^+ = Q_{\text{adv}}^- + F_{\text{rad}}^-, \quad (5)$$

here, Q_{vis}^+ is the viscous heating rate per unit surface, F_{rad}^- is the radiative cooling term, and Q_{adv}^- is the effective cooling induced by heat advection. They can be specified as follows:

$$Q_{\text{vis}}^+ = -\frac{1}{4\pi r} \frac{\gamma_{\phi} A^{1/2}}{\Delta^{1/2} r} \dot{M} (L - L_{\text{in}}) \frac{d\Omega}{dr}, \quad (6)$$

$$\begin{aligned} Q_{\text{adv}}^- &= -\frac{\dot{M}}{4\pi r} \frac{W}{\Sigma} \frac{1}{\Gamma_3 - 1} \left(\frac{d \ln W}{dr} - \right. \\ &\quad \left. \Gamma_1 \frac{d \ln \Sigma}{dr} - (\Gamma_1 + 1) \frac{d \ln H}{dr} \right), \end{aligned} \quad (7)$$

where Γ_1 and Γ_3 are defined in Kato et al. (1998), and

$$F_{\text{rad}}^- = \frac{8acT^4}{3\kappa\rho_0 H}. \quad (8)$$

The Rosseland mean of total opacity can be expressed as

$$\kappa = 0.4 + 0.64 \times 10^{23} \rho T^{-7/2}.$$

The total pressure can be expressed as the sum of the gas and radiation pressure. For simplicity, we drop the numerical factors in Shimura & Manmoto (2003), and the equation of state is given by:

$$W = \frac{1}{3}aT^4H + \frac{2k_B}{m_p}\Sigma T, \quad (9)$$

where T is temperature of the disk. Another equation is the vertical thickness equation, which reads

$$H = \sqrt{12} \frac{c_s}{\Omega_k} g_{\text{pa}}^{-\frac{1}{2}}. \quad (10)$$

This is a modification to the equations of Shimura & Manmoto (2003), and its derivation will be presented in Section 2.2.

The above equations are transformed into a set of first-order differential equations with variables v_r and W , and then integrated from the outer boundary at about $10^5 r_g$.

The transonic solutions (Liang & Thompson 1980) are obtained using a shooting method, in which we adjust L_{in} recursively until the smooth transonic solution is found. During the solving process, despite that the factor g_{pa} takes form

$$g'_{\text{pa}} = \gamma_\phi^2 \left(\frac{(r^2 + a^2)^2 + 2\Delta a^2}{(r^2 + a^2)^2 - \Delta a^2} \right), \quad (11)$$

a simplified version of factor g_{pa} is used when finding the global transonic solution:

$$g_{\text{pa}} = \frac{(r^2 + a^2)^2 + 2\Delta a^2}{(r^2 + a^2)^2 - \Delta a^2}. \quad (12)$$

However, the location of the photosphere (Peitz & Appl 1997) is still determined according to Equation (13). When this simplification is taken, at the inner regions of the accretion disks, the resulting disk photosphere and disk thickness no longer agree with each other. But the difference is not significant. We thus neglect this inconsistency and use the location of the disk photosphere in the ray-tracing calculation.

2.2. Estimation of the Vertical Thickness

The vertical thickness is a major uncertainty in the accretion disk theory, and is claimed to be dependent on various physical assumptions such as the vertical dissipation profiles and the interplay between the relaxation time scale and the free-fall time scale. However, Sadowski et al. (2009) showed that the vertical thickness of an accretion disk in the non-advective regime can be approximated using this simple formula:

$$\kappa \sigma T_{\text{eff}}^4 \frac{1}{c} = \frac{2}{3} \Omega_k^2 z g_{\text{pa}}, \quad (13)$$

where κ is the total opacity, σ is Stefan–Boltzmann constant and z is the photosphere location. T_{eff} is the effective temperature defined as $T_{\text{eff}} = (F_{\text{rad}}^-/\sigma)^{1/4}$ and $\Omega_k = r^{-3/2}$. Equation (13) simply means that at the disk photosphere, the vertical radiation pressure balances the gravity of the central black hole. In this work, despite the fact that Equation (13) has only been shown to be valid in the non-advective regime, we also use it in the advective regime, since the physical argument is still valid. With this assumption, we can get the expression for the location of the photosphere:

$$z = \kappa \frac{3\sigma T_{\text{eff}}^4}{2\Omega_k^2 g_{\text{pa}}} \frac{1}{c} = \frac{3}{2} \kappa \frac{F_{\text{rad}}}{c} \Omega_k^{-2} g_{\text{pa}}^{-1}. \quad (14)$$

Another constraint comes from the vertical radiation flux. According to the diffusion approximation, assuming the dominance of the radiation pressure, the radiation flux can be approximated as

$$F_{\text{rad}} = \frac{8acT^4}{3\kappa\rho_0 H} = \frac{8cW}{\kappa\Sigma H}. \quad (15)$$

We thus make the physical requirement that the thickness z obtained in Equation (14) should be consistent with the thickness H in Equation (15). Combining these two equations, we obtain the expression for modified disk thickness:

$$H = \sqrt{12} \frac{c_s}{\Omega_k} g_{\text{pa}}^{-\frac{1}{2}}. \quad (16)$$

It should be noted that Equation (16) is accurate when the disk is radiation pressure dominated. At the outer regions of the accretion disks, where the gas pressure dominates, Equation (16) deviates from the previous one by a factor of $\sqrt{12}$ (the previous expression takes form $H = c_s/\Omega_k g_{\text{pa}}^{-1/2}$). However, as Sadowski et al. (2009) showed, the thickness in the outer region of the accretion disks is not well constrained, and it is dependent on the dissipation profile in the vertical direction. As the contribution of radiation from the gas-dominated region is relatively unimportant and the final emergent SED is unaffected by our modifications significantly, we use Equation(16) throughout the paper. One concern about the estimation of thickness is that the effect of magnetic field may influence the disk thickness. Hirose et al. (2006) pointed out that the location of photosphere of the accretion disk is modified by the magnetic field significantly. However, in our case, the shadowing effect happens at the inner region, where the radiation pressures dominates. Thus the thickness and the self-shadowing might not be significantly affected by the magnetic effect. The magnetic field might also change the inner boundary condition significantly (e.g. Penna et al. 2010; Noble et al. 2010, and references therein). To investigate the effects of the magnetic field, we should do the general relativistic MHD simulations (Gammie et al. 2003; De Villiers et al. 2003), which is beyond the scope of this work.

2.3. Ray-Tracing Method

After obtaining the global structure of the relativistic disk, we use the ray-tracing technique to calculate the emergent spectra with inclusion of all the relativistic effects. The ray-tracing method is based on the analytical integration of the null-geodesics (Chandrasekhar 1983; Rauch & Blandford 1994; Cadez et al. 1998), and the subroutines are the same as those used in Yuan et al. (2009).

One major improvement compared to earlier work (e.g. Li et al. 2005) is that we include the disk thickness in the ray-tracing calculation. To achieve this, we start from the infinity, and then search along the each photon trajectory for the intersection point.

Once the intersection points are found, we can calculate the local temperature of the emitting points in our disk model and calculate the redshift factor g . The emergent spectra are then obtained by integrating over the photometric plane according to

$$F_{\nu_o} = \int g^3 I_{\nu_e} \frac{d\alpha d\beta}{D^2}, \quad (17)$$

where α and β are two impact parameters, and the redshift

factor is

$$g = \frac{\nu_o}{\nu_e}, \quad (18)$$

here D is the distance of the object expressed in geometrical units and I_ν takes the diluted blackbody form (e.g., Shimura & Takahara 1995).

The redshift factors are calculated as follow:

$$g = \frac{\nu_{\text{obs}}}{\nu_{\text{em}}} = \frac{p_\mu u_{\text{Observer}}^\mu|_{r=\infty, \theta=\theta_{\text{obs}}}}{p_\mu u_{\text{Fluid}}^\mu|_{r=r_{\text{em}}, \theta=\theta_{\text{em}}}}, \quad (19)$$

where p_μ is the four-momentum of the photon, given by Carter (1968)

$$p_\mu = (-1, \pm \frac{\sqrt{R}}{\Delta}, \pm \Theta^{1/2}, \lambda). \quad (20)$$

The four-velocity of the fluid is given by Yuan et al. (2009)

$$u_{\text{Fluid}}^\mu = (\gamma_r \gamma_\phi e^{-\nu}, \gamma_r \beta_r e^{-\mu}, 0, \gamma_r \gamma_\phi (\omega e^{-\nu} + \beta_\phi e^{-\psi})), \quad (21)$$

where $e^\nu = (\Sigma \Delta / A)^{1/2}$, $e^\psi = (A \sin^2 \theta / \Sigma)^{1/2}$. Thus we have the expression for redshift factor:

$$g = \frac{\Sigma^{1/2} \Delta^{1/2}}{A^{1/2}} \frac{1}{\gamma_r \gamma_\phi} \frac{1}{1 \mp \frac{\beta_r R^{1/2}}{\gamma_\phi A^{1/2}} - \lambda \omega - \lambda \beta_\phi \frac{r^2 \Delta^{1/2}}{A}} \quad (22)$$

where ‘‘em’’ means the emitting points, and the ‘‘+’’ sign for the trajectories of the photons without r -turning point and ‘‘-’’ sign for those with r -turning point. In Equation(20),

$$R = r^4 + (a^2 - \lambda^2 - Q)r^2 + 2(Q + (\lambda - a)^2)r - a^2 Q. \quad (23)$$

here the definition of λ and Q are the same as that of Cunningham & Bardeen (1973).

In the ray-tracing calculations, the outer boundary condition of the integration is set at $10^5 r_g$. In the cases when the emitting radius is so large that the disk solutions do not cover, we use the results from SSD instead, because the differences between the transonic disk model and SSD are indeed insignificant at the large radii.

One limitation in our calculation is that the returning irradiation (van Paradijs & McClintock 1995; Li et al. 2005) is neglected. In the inner regions of the accretion disk, due to the strong gravity, the radiation emitted at one part of the accretion disk may reach other parts, which may result in a modification to the disk structure and the emergent spectra. Certain disk geometry may enhance such kind of effect (van Paradijs & McClintock 1995). In the case of the thin accretion disk, this effect has moderate influence (about several percents) on the emergent spectra (Li et al. 2005). In our case, due to the thick geometry, since the disk is shadowed by itself, the self-irradiation effect may be stronger. As the inclusion of that effect requires significant amount of calculation, for simplicity, we neglect it in our current work.

Another limitation in our calculation is that the effect of limb-darkening has not been considered. As Li et al. (2005) have pointed out, the limb darkening has effect on the emergent spectra, especially when the inclination angle is large, and the deviation induced by this effect is about 10% at low energy band when the disk is viewed at 85° (Li et al. 2005). In this work, this effect has not been included. According to the limb-darkening law $I_\theta \sim 1/2 + 3/4 \cos \theta$, our results are still robust at relatively small inclination angles.

3. STRUCTURE OF THE RELATIVISTIC DISK

We present our results on the structure of the accretion disk. Throughout this paper, the critical accretion rate is taken as

$$\dot{M}_{\text{edd}} = 16 \frac{L_{\text{edd}}}{c^2}, \quad (24)$$

where the numerical factor comes from the energy generation efficiency of the Schwarzschild black hole. For the sake of comparison, we adopt the same critical accretion rate for both the Schwarzschild and Kerr black holes. This is different from the convention used in McClintock et al. (2006). Similar results have already been obtained by Sądowski (2009), and one major difference between our work and theirs is that our work is based on a different estimation of the vertical thickness.

In our canonical model, the mass of the black hole is taken to be $10M_\odot$, while the viscosity coefficient α is set to be 0.1. The dimensionless accretion rates are taken to be 1/4, 1/2, 1 and 2 respectively, ranging from the sub-Eddington systems to the moderate super-Eddington ones. A special case for the low accretion rate $\dot{M} = 1/16$ is also discussed when $a = 0.98$.

3.1. Disk Dynamics

Figures 1-3 show the dynamical properties of our accretion disks. The upper panels in Figure 1 show the radial velocity as a function of radii, with the different accretion rates. Because we use fully relativistic equations, near to the event horizon of the black hole, as expected, the radial velocity is very close to the speed of light. At the small radii, for the same accretion rate, the higher the spin, the smaller the radial velocity. At the large radii, the radial velocity of the accretion flow is relatively small, and it is insensitive to the black hole spin. This is because that at the large radii, the disk structure resembles that of SSD. With the increase of the accretion rate, the radial velocity becomes larger.

The lower panels of Figure 1 show the radial distribution of the surface density under the different accretion rates. Generally speaking, at the small radii, the surface density is small. These results can be simply understood in terms of the non-relativistic form of the matter conservation:

$$\dot{M} = 2\pi r \Sigma v_r,$$

where Σ is the surface density of the accretion disks, and v_r is the radial velocity (the relativistic one is similar but with an additional corrections related to the radial Lorentz factor γ_r and the black hole spin a). Since the accretion disks around Schwarzschild black holes tend to have higher radial velocity, their surface density at given radius is smaller. Another noticeable feature is that the density hop occurs when $\dot{M} = 0.25 \dot{M}_{\text{edd}}$, $a = 0$, which is accompanied by the velocity decrease and re-increase in the upper panels. This peculiar behavior is not shown in Shimura & Manmoto (2003) since they did not explore the disk solution at such a low accretion rate, but can be found in the previous papers solving the non-relativistic slim disk structure (Chen & Wang 2004) and a recent relativistic one (Sądowski 2009, with explanation).

Upper panels of Figure 2 show the rotation velocity of the accretion flow. The rotation velocity is insensitive to the accretion rate, especially at the outer region. To show how the fluid motion deviates from the Keplerian motion, the ratio of the rotational velocity to the rotational velocity of the Keplerian motion $v_\phi / v_\phi^{\text{Kep}}$ are shown in the lower panels of Figure

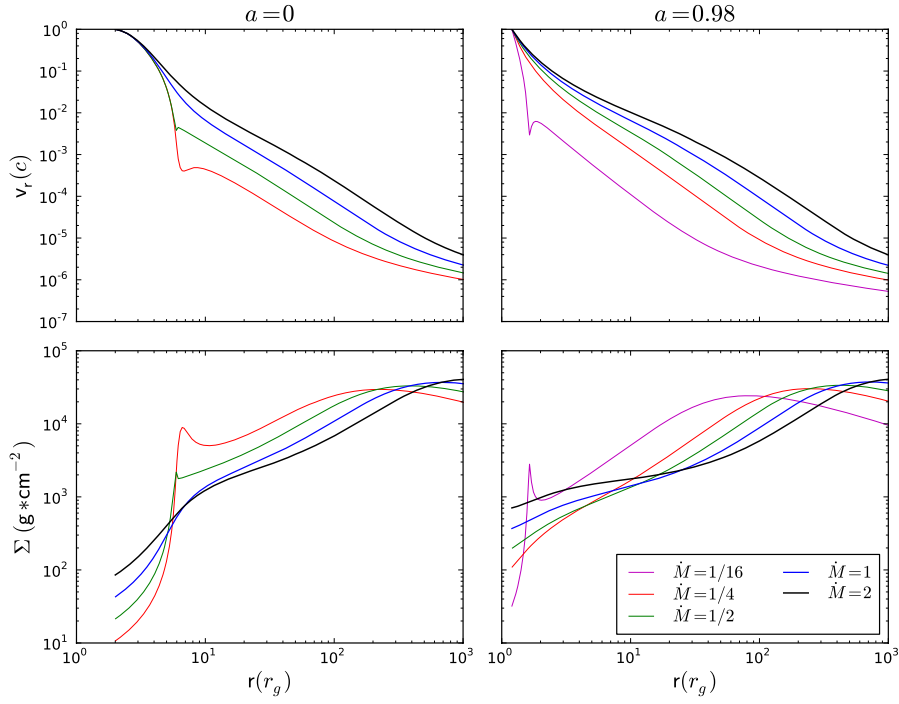


FIG. 1.— Radial velocity and surface density as a function of radii. From thin to thick, the lines stand for the solutions for the accretion rates $1/16\dot{M}_{\text{edd}}$, $1/4\dot{M}_{\text{edd}}$, $1/2\dot{M}_{\text{edd}}$, $1\dot{M}_{\text{edd}}$ and $2\dot{M}_{\text{edd}}$ respectively. The left panels correspond to Schwarzschild black hole, and the right panels correspond to Kerr black hole with $a = 0.98$. The black hole mass is taken to be $10M_{\odot}$.

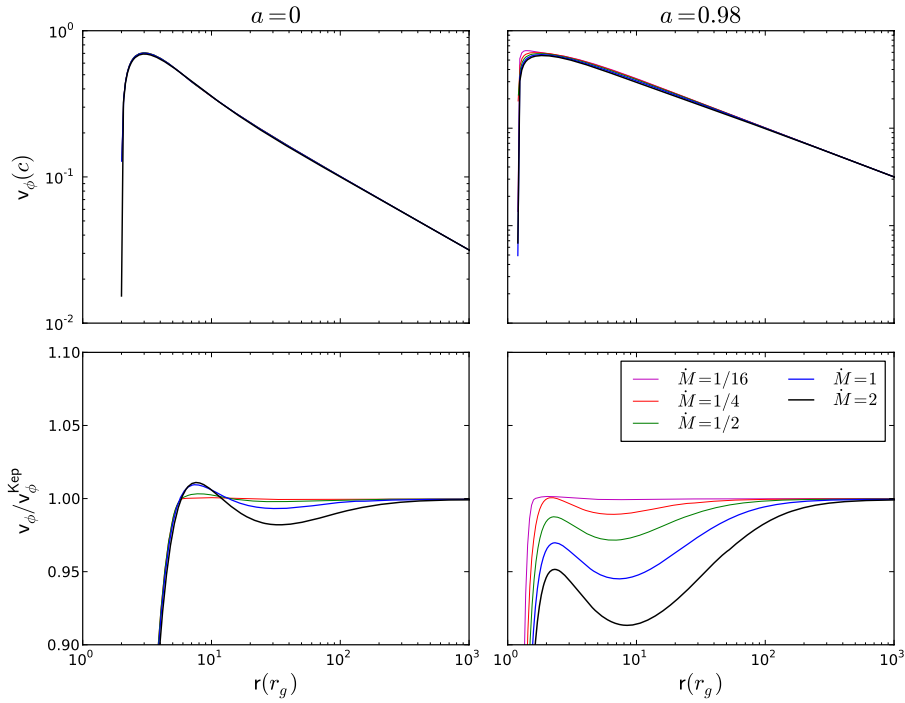


FIG. 2.— Rotation velocity and the ratio of rotation velocity to Keplerian rotation velocity $v_{\phi}/v_{\phi}^{\text{Kep}}$ vs. radii. The symbols of the lines are the same as in Figure 1. The left panels correspond to Schwarzschild black hole, and the right panels correspond to Kerr black hole with $a = 0.98$.

2. When the accretion rate is low, the rotation velocity ratio is very close to unity, which means the assumptions made in SSD are accurate. When the accretion rate is relatively high, the rotation of the fluid becomes sub-Keplerian. In some regions, the rotation is super-Keplerian. Although there exists some differences, the deviation is no more than 10% at several gravitational radii, which means the assumption of the Keplerian motion is still valid at the most of the regions of the accretion disks (see e.g. Igumenshchev & Abramowicz 2000).

Figure 3 shows the effective temperature T_{eff} as a function of radii. Here, T_{eff} is defined as $T_{\text{eff}} = (F_{\text{rad}}^-/\sigma)^{1/4}$, where F_{rad}^- is the radiation flux per unit area and σ is the Stefan–Boltzmann constant. Similar to the above figures, the differences between the Schwarzschild and the Kerr black holes are all very small at large radii. With the increase of the accretion rate, the temperature increases. When the accretion rate is high enough, the temperature is still high even inside the ISCO, which suggests that, contrary to the assumptions made in the SSD model, the matter inside the ISCO is not cold.

3.2. Disk Thickness

Figure 4 shows the thickness of the disk vs. the radii. In order to give a instinctive picture of the disk thickness, we use linear coordinate, and show only the results in the inner part of the accretion disk. This thickness profile is thus correspond to the surface of the accretion disk. The imprints of ISCO appear in the disk thickness profile. This feature is particularly prominent at low accretion rate, where the disk surface agrees with the simulation carried out by Hawley & Krolik (2002) and Reynolds & Fabian (2008). When the accretion rate is high enough, the imprints of ISCO disappear, and the disk shows a continuous profile down to the event horizon of the black hole.

However, in some cases, the estimation of thickness may be incorrect. Since the estimation of the thickness is based on the vertical *hydrostatic* equilibrium, it depends on the assumption:

$$a_z^{\text{Fluid}} < g_z, \quad (25)$$

which means the acceleration in the vertical direction could never exceed the acceleration provided by the vertical gravitational force (or that the disk has time to relax to the hydrostatic equilibrium). We checked our solutions using this formula, and found that in some cases such as $\dot{M} = 0.25$, $a = 0$ Equation (25) is not satisfied. Thus the disk thickness may be under-estimated at the regions near ISCO, in some cases.

3.3. Energy Dissipation Inside ISCO

In Figure 5, we present our results on the global energy balance of the accretion disks. The energy conservation in the accretion disks takes the simple form as follows:

$$Q_{\text{vis}}^+ = F_{\text{rad}}^- + Q_{\text{adv}}^-, \quad (26)$$

where Q_{vis}^+ is the viscous energy generation rate, F_{rad}^- is the cooling term due to radiation from the accretion disk, and Q_{adv}^- is the effective cooling induced by the heat advection. If $Q_{\text{vis}}^+ \sim F_{\text{rad}}^-$, the disk is very similar to the standard accretion disk since the energy generated by the viscous processes is radiated locally. If $Q_{\text{vis}}^+ \sim Q_{\text{adv}}^-$, most of the heat generated is trapped inside the accretion disk.

Figure 5 shows the ratio of the emitted radiation from the disk surface to the total heat generated by the viscous processes. At about $20 r_g$, the heat advection works, as a result,

the ratio is less than 1. However, in the inner region, in many cases, F_{rad}^- dominates over Q_{vis}^+ , which means that substantial amount of energy is still being radiated away. The source of the energy mainly comes from the energy trapped in the region outside the ISCO. Thus our results suggest that the radiation trapped outside the ISCO can be allowed to escape at the regions close to the black hole. This kind of mechanism is new, since different from the advective cooling, in some cases, the effect of advection will heat the disk up, resulting in “advective heating”.

Besides from getting self-consistent disk solution, we find that when the accretion rate is low enough such as $\dot{M} \sim 1/4$ for $a = 0$ and $\dot{M} \sim 1/16$ for $a = 0.98$, the SSD model is valid.

4. EMERGENT SPECTRA

We present the resulting emergent spectra based on the ray-tracing method. We assume that the local emission of the disk takes the diluted blackbody form with the spectra hardening factor equals 1.7 (Ross et al. 1992; Shimura & Takahara 1993, 1995), which is actually dependent on disk luminosity as shown in Davis et al. (2005) and Done & Davis (2008).

To show the effect of the photon trapping and the disk thickness, we consider three cases. In the first case (case A), we calculate the spectra from the relativistic standard accretion disks. In this case, our spectra are completely identical to the spectra generated by KERRBB with exactly the same parameters. In the second case (case B), we calculate the spectra from the relativistic slim accretion disks, assuming that the disk is still geometrically thin. This is for the purpose of showing the effect of the heat advection, the sub-Keplerian motion, the radial plunging and the radiation from the plunging region. In the third case (case C), based on case B, we consider the effect of disk thickness to show the disk self-shadowing.

The emergent spectra are shown in Figure 6. The differences between case A (black solid line) and case B (blue dotted line) are due to the combination of the effects of the photon trapping, the radiation from the plunging region and the motion of the fluid. The effect of the motion of the fluid on the emergent spectra is determined mainly by the Lorentz factors, γ_r , γ_ϕ . At the ϕ direction, the velocity differences between the slim disk model and the thin, Keplerian SSD model is relatively small, thus the effect is not significant. At the r direction, the radial velocity works. Since matter plunges into the black hole, in most cases, this will introduce a net redshift. At some rare cases where the photon trajectories have r turning points (e.g. Cadez, Fanton, & Calvani 1998), the radial velocity field will introduce net blue-shift. But this blue shift is usually unimportant since this kind of trajectory is rare. The radial velocity effect is significant only near or inside the ISCO.

The other important effect is the photon trapping. Since the previous works focus on the application of slim disk model in the highly accreting systems, the effects of the photon trapping in their cases are thus to bring down the luminosity, and highly attenuate the flux at the high energy band. However, for the relatively low accretion rate, the photon trapping behaves quite differently. In fact, contrary to the previous view that photons are trapped and not allowed to radiate away, substantial amount of trapped photons is allowed to re-radiate in the plunging region where the energy dissipation is relatively insignificant. This effect will in fact distort the spectrum and hence affect the spin measurement. This phenomenon is com-

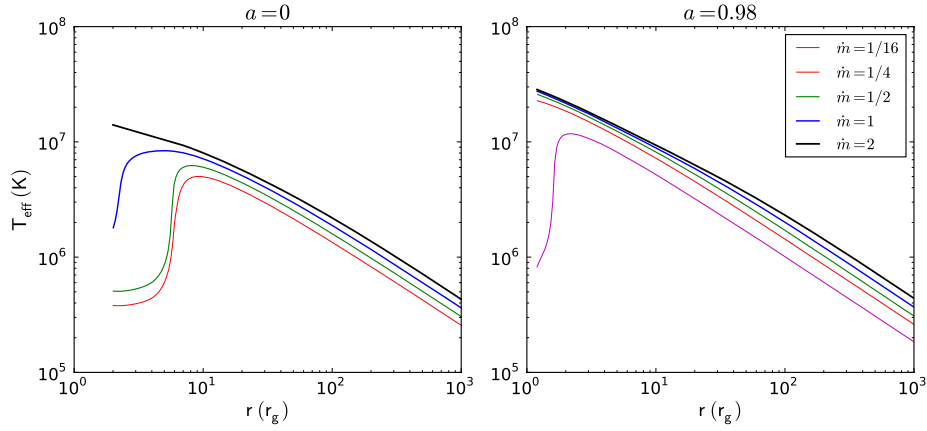


FIG. 3.— Effective temperature T_{eff} vs. radii r . The symbol of the lines are the same as in Figure 1. The left panels correspond to the Schwarzschild black hole, and the right panels correspond to the Kerr black hole with $a = 0.98$.

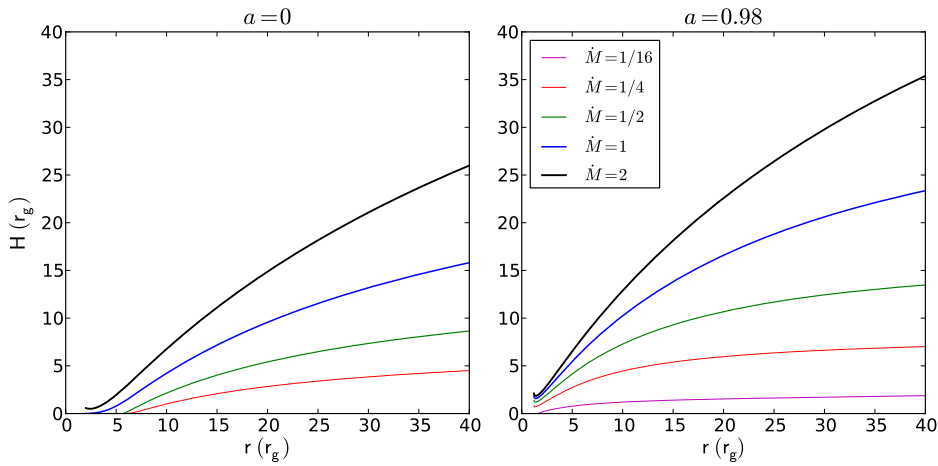


FIG. 4.— Vertical thickness as function of radius. The symbol of the lines are the same as in Figure 1. The left panels correspond to the Schwarzschild black hole, and the right panels correspond to the Kerr black hole with $a = 0.98$.

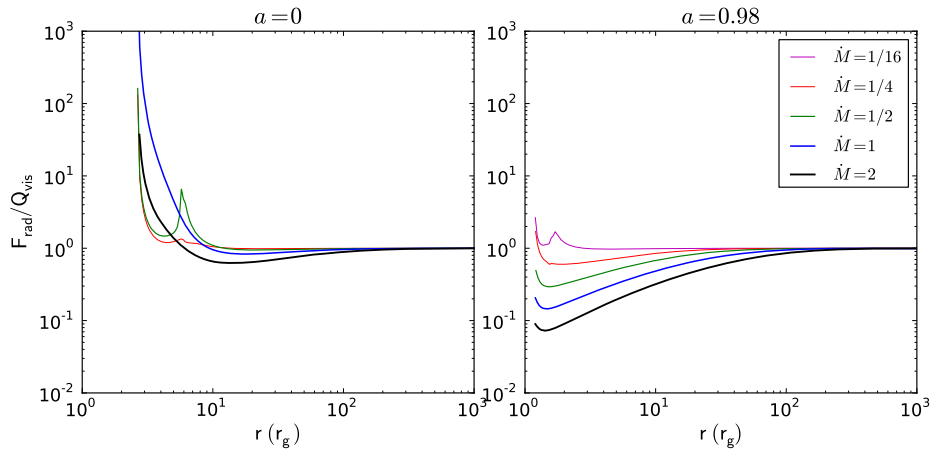


FIG. 5.— $\frac{F_{\text{rad}}}{Q_{\text{vis}}}$ as function of r . The symbol of the lines are the same as in Figure 4.

mon for both the non-rotating and rotating black hole systems when the accretion rate is moderate.

The differences between case B and case C are due to the inclusion of the thickness of the disk in our calculations. It is clearly seen that the inclusion of the effect of the disk thickness will bring down the flux, especially at high energy band, and is more prominent at the higher accretion rate, higher inclination angle and larger spin. When the accretion rate increases, the disk thickness increases, and the self-shadowing happens at a relatively small inclination angle. For the Kerr black hole, since the energy generation rate is higher, the disk self-shadowing effect is more prominent.

Since the differences between case A and case B are what referred to as the photon trapping effect, the differences between case B and case C are due to the effect of the disk self-shadowing, which has never been worked out before. In fact, when the accretion rate is high, the effect of the disk self-shadowing is more significant than that of the photon-trapping effect alone. Thus, in order to study the spectra from the super-critical accretion disks, we have to consider those two effects simultaneously.

According to our results, for the disk around a Kerr black hole with $a = 0.98$, if the disk inclination is 60° , at about 0.23 of Eddington luminosity, the effects of the heat advection and disk self-shadowing begin to be important. Although in our case (the bottommost set of curves in Figure 6), the effects of the heat advection and disk self-shadowing tend to cancel each other, our results set a critical luminosity beyond which the relativistic standard accretion disk model is no longer applicable for the spectra fitting.

5. ANGULAR DEPENDENCE OF THE LUMINOSITY

We explore the angular dependence of the disk luminosity. In the case of a thin slab of the stationary gas, the angular dependence of emergent luminosity should be $L \sim \cos \theta$. In the case of an accretion disk, the angular dependence of the disk luminosity $L(\theta)$ is also influenced by several other effects, including the disk geometry and the disk rotation. In Figures 7-8, we show both the luminosity in the X-ray band ($0.1 \sim 100\text{KeV}$), which is of observational interest, and the total luminosity.

Figure 7 shows the luminosity in the X-ray band as a function of the inclination. The upper panels show the results for a non-spinning black hole, and the lower panels show the spectra for a spinning black hole with $a = 0.98$. For the standard accretion disk model, the angular dependence of the luminosity deviates from $L \sim \cos \theta$ due to the Doppler shift induced by motion of the fluid. For the disk around a Schwarzschild black hole, the effect of the Doppler shift tends to flatten the profile, which means that the radiation is more weakly beamed than that of a single slab, for the disk around a Kerr black hole, this effect is so strong that the angle at which luminosity peaks is not 0° .

The dotted lines in the subpanels of Figure 7 show the angular dependence of the X-ray luminosity for a dynamical thin accretion disk which is different from the standard accretion disk since its velocity field is different and the photon trapping effect is taken into account. For the low accretion rate, as we have discussed, the effect of photon trapping is complicated. For the high-enough accretion rate, the effect of heat advection will highly attenuate the total luminosity.

The solid lines in the subpanels of Figure 7 show the angular dependence of X-ray luminosity for a dynamical thick accretion disk. Compared to the blue dotted lines, the effect

of disk thickness is taken into account. In all cases, the inclusion of disk thickness tends to attenuate the radiation, even in the face-on case, since light is bend by the strong gravity. Another difference caused by the disk thickness is a mild beaming of radiation (e.g. Heinzeller et al. 2006), which means that the disk is more luminous when viewed face-on than viewed edge-on.

The angular dependence of the total luminosity is shown in Figure 8. The trend is similar to the previous figure. However, the effect of the motion of the fluid is relatively weak. The reason is that in calculating the X-ray luminosity, the low-energy photons can be Doppler boosted into the X-ray band and contributed to the X-ray luminosity. However, that effect will not significantly influence the total luminosity.

The mass of the black hole in our model is taken to be $10M_\odot$. Since the disk thickness in the inner regions of the accretion disks is dependent on the accretion rate but independent of black hole mass (Kato et al. 1998; Watarai 2006), for a given θ_{crit} , the effect of self-shadowing is only a function of the black hole accretion rate. Given the same Eddington-scaled luminosity, since the other physical parameters such as T (the temperature or equivalently the characteristic frequency) and L_{tot} (the normalization of the flux) scale as

$$T \sim M^{-\frac{1}{4}} \quad (27)$$

$$L_{\text{tot}} \sim M, \quad (28)$$

our results can be scaled to a considerable range of parameters, and then can be used to fit the observational results of the supermassive black holes.

6. IMPLICATIONS FOR SPIN MEASUREMENT

TABLE 1
PARAMETERS OF KERRBB

Parameters Name	Description	Value	Freeze
η	Inner torque	0	Yes
M_{bh}	Mass of black hole	10	Yes
θ_{obs} (degree)	Disk inclination angle	30, 60 ^a	Yes
D (kpc)	Distance	10	Yes
rflag	Self-radiation	0	...
lflag	Limb-darkening	0	...
f_{col}	Spectral hardening factor	1.7	Yes
K	Normalization	1	Yes
\dot{M}	Accretion rate	...	No
a	Spin	...	No

^aThe values used in the fittings are the same as the value used in producing the spectra

We show how the different SEDs in different models affect the measurement of the black hole spin. To achieve this, we create “fake” data sets from our spectra by convolving with a response matrix of XMM-NEWTON using XSPEC (Arnaud 1996) version 12.5. The “faked” data sets are then fitted with the KERRBB model in XSPEC.

The KERRBB model is a publicly available XSPEC model that can be used to calculate the multicolor disk (MCD) spectra of a relativistic, thin accretion disk around a Kerr black hole. The model settings in our fittings are summarized in Table 1. Our fitting strategy is similar to that of Shafee et al. (2006). The differences are that we turn off the limb-darkening and self-radiation, and we always set the spectral hardening factor f_{col} to be 1.7. This is because we require the fittings consistent with the assumptions in our model.

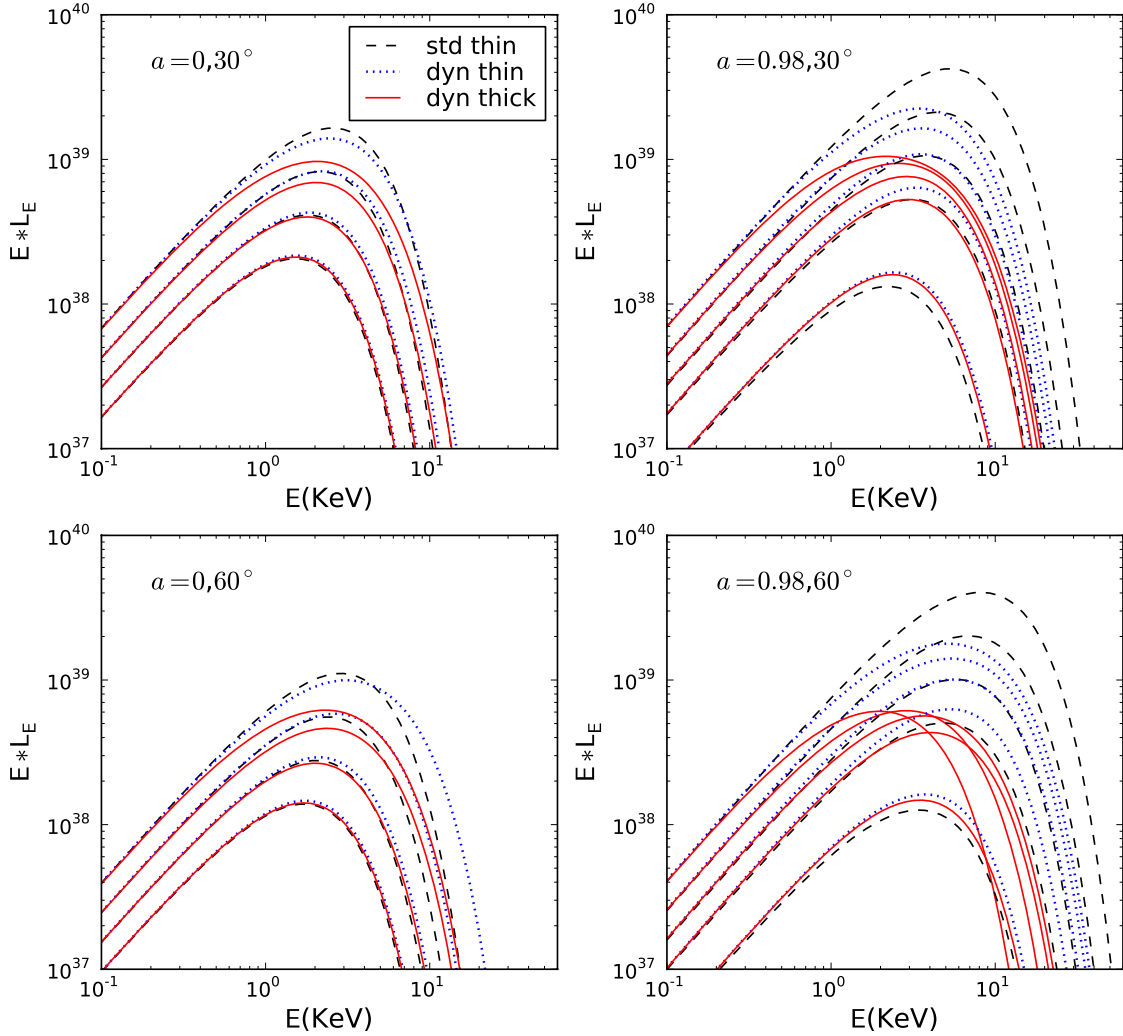


FIG. 6.— The emergent spectra. The upper panels show the spectra when the disk is viewed at 30° , while the lower panels show the spectra at 60° . The left panels show the spectra from the non-spinning black holes ($a = 0$), the right panels show the spectra from the spinning black holes ($a = 0.98$). The black dashed lines correspond to the spectra from the relativistic standard disks (case A), the blue dotted lines correspond to the spectra from the relativistic slim accretion disks with no thickness (case B), and the red solid lines correspond to the spectra from the relativistic slim accretion disks with the inclusion of thickness effect (case C). The accretion rate takes the values: $1/4 M_{\text{edd}}$, $1/2 M_{\text{edd}}$, $1 M_{\text{edd}}$, $2 M_{\text{edd}}$ (left panels, $a = 0$) and $1/16 M_{\text{edd}}$, $1/4 M_{\text{edd}}$, $1/2 M_{\text{edd}}$, $1 M_{\text{edd}}$, $2 M_{\text{edd}}$ (right panels, $a = 0.98$) respectively. The black hole mass is taken to be $10 M_\odot$.

The fittings are carried out by making our calculated spectra into a table model, then the faked data can be easily generated using the *fakeit* command. The faked spectra are then fitted to model KERRBB with the procedure described above. The fittings are robust in the sense that the different initial values of black hole spin a and the accretion rate \dot{M} lead to almost the same results.

Figure 9 shows the measured spin. For the moderate accretion rate, the effect of the heat advection alone leads to the overestimation of black hole spin, while for the high-enough accretion rate, this usually leads to the underestimation of the black hole spin. This is true for both the Schwarzschild and Kerr cases, and for the Kerr case these phenomena occur at a relatively lower accretion rate. The effect of the disk thickness will always lead to the under-estimation of black hole spin and is very significant when the accretion rate, the inclination or the spin, is large. Combining these two effects, in most cases, we generally underestimate the black hole spin. Only when the physical parameters are appropriate, we can obtain a overestimation of the black hole spin.

7. DISCUSSIONS

7.1. Shadowing Effect Enhanced by the Strong Gravity

It is of theoretical interest to investigate what influences the effect of the self-shadowing. Without the light-bending effect, the self-shadowing effect is dependent on the maximum of H/r , which is mainly dependent on the black hole accretion rate (McClintock et al. 2006). However, it remains unclear how the shadowing effect influenced by the strong gravity.

To gain physical insight into this question, we choose two systems with exactly the same luminosity but the different spin (one with $\dot{M} = 1$ and $a = 0.974$, another with $\dot{M}=4$ and $a = 0$), and calculated the spectra. For both systems, we calculate the spectra both with and without the effect of light-bending. In the latter case, for self-consistency, the redshift is evaluated as

$$g = \frac{\Delta^{1/2}r}{\gamma_r \gamma_\phi A^{1/2}} \frac{1}{1 \pm \frac{\beta_r \sqrt{R}}{\gamma_\phi A^{1/2}} - \Omega \lambda}. \quad (29)$$

After that, to quantify the effect of disk self-shadowing, we compare the SED calculated with disk thickness and the SED calculated without disk thickness by defining the spectral distortion as function of frequency as

$$\text{Distortion}(\nu) = \frac{\text{SED}_{\text{not shadowed}} - \text{SED}_{\text{shadowed}}}{\text{SED}_{\text{not shadowed}} + \text{SED}_{\text{shadowed}}}, \quad (30)$$

where the $\text{SED}_{\text{not shadowed}}$ denotes the SED calculated by assuming slim disk with no thickness, and $\text{SED}_{\text{shadowed}}$ denotes the SED calculated including the disk thickness.

The spectral distortion for different spin and different assumptions about light trajectories is plotted in Figure 10. For both the Schwarzschild and the Kerr black hole, including the light bending effect brings about significant distortion to the emergent spectra, and this distortion generally appears as attenuation of the flux at high energy part. This kind of distortion is more significant for Kerr black hole, because the light trajectories are more severely influenced by the strong gravity.

7.2. Diversity in Spectral Evolution

It was known that the spectral evolution of the X-ray binary deviates from the trend predicted in the SSD model

at both the low and high luminosities (Done et al. 2007; Kubota & Makishima 2004). Although the deviation at the low luminosity states is often interpreted as the evaporation (Meyer & Meyer-Hofmeister 1994) of the optically thick disk into the optically thin ADAF (Advection Dominated Accretion Flow, Narayan et al. 1997; Narayan & Yi 1995, 1994), the deviation at the high luminosity states is still mysterious.

The standard accretion disk model predicts the monotonic evolution of the disk peak energy with the luminosity, i.e., the higher peak energy corresponds to the higher luminosity. This kind of spectral evolution is consistent with the spectra evolution of X-ray binary at the medium luminosity states. However, beyond some critical luminosity L_{crit} the peak of the disk SED shifts to the low energy band (Done et al. 2007), with the increase of the disk luminosity. This kind of spectral evolution is difficult to be understood in the SSD model.

To tackle this problem, various attempts have been made, which include a change of the color correction with the luminosity (Davis et al. 2006) as well as the effects of the optically thick advection. One common difficulty with these explanations is that they all predicts a single critical luminosity L_{crit} , which is in contradiction with the diversity of the critical luminosity observed in the different sources (Done et al. 2007).

One natural explanation from our calculations is that the abnormal of the spectral evolution is due to the self-shadowing of the accretion disks. The trend of the observed spectral evolution is consistent with our results as shown in Figure 6, and the diversity of the critical luminosity $L_{\text{disk}}/L_{\text{edd}}$ in the different sources might be due to the different inclination angle and black hole spin. According to our results, the critical luminosity becomes smaller for the larger inclination angle or the black hole spin.

Our results also provide a diagnostic of the location of the shadowing medium. If the shadowing happens at the inner region of the accretion disks, the critical luminosity is dependent on black hole spin as well as the inclination angle. If the disk is shadowed by the matter distant from the black hole, (e.g., equatorial wind; (Done & Davis 2008)), the critical luminosity is dependent only on the black hole spin.

7.3. The Spin of GRS 1915+105

The spin of GRS 1915+105 is debated in the literature. By fitting the disk blackbody component, McClintock et al. (2006) found that the spin is near extreme, while Middleton et al. (2006) found the spin is moderate, with $a \sim 0.8$. One major difference between these two works is that the spin obtained by McClintock et al. (2006) is based on the spectra fitting for the relatively low luminosity ($L < 0.3L_{\text{edd}}$) states, while Middleton et al. (2006) set no strict restriction on the luminosity states. Interestingly, McClintock et al. (2006) found that the measured spin becomes smaller for the higher luminosity states.

To show how the spin can be recovered by the fitting procedure, we simulate the artificial data in our model which is added with comptonization model *comptt* (Titarchuk 1994), iron absorption edge, iron absorption line as well as galactic absorption, and then we fit the data with the same procedure as used in McClintock et al. (2006). All the parameters are the same as those in McClintock et al. (2006). The only difference in the artificial spectral fitting is that we replace the KERRBB2 model with KERRBB model, and set the spectral hardening factor to be 1.7.

Our results are shown in Figure 11. Without introducing the additional parameters, we are able to roughly reproduce

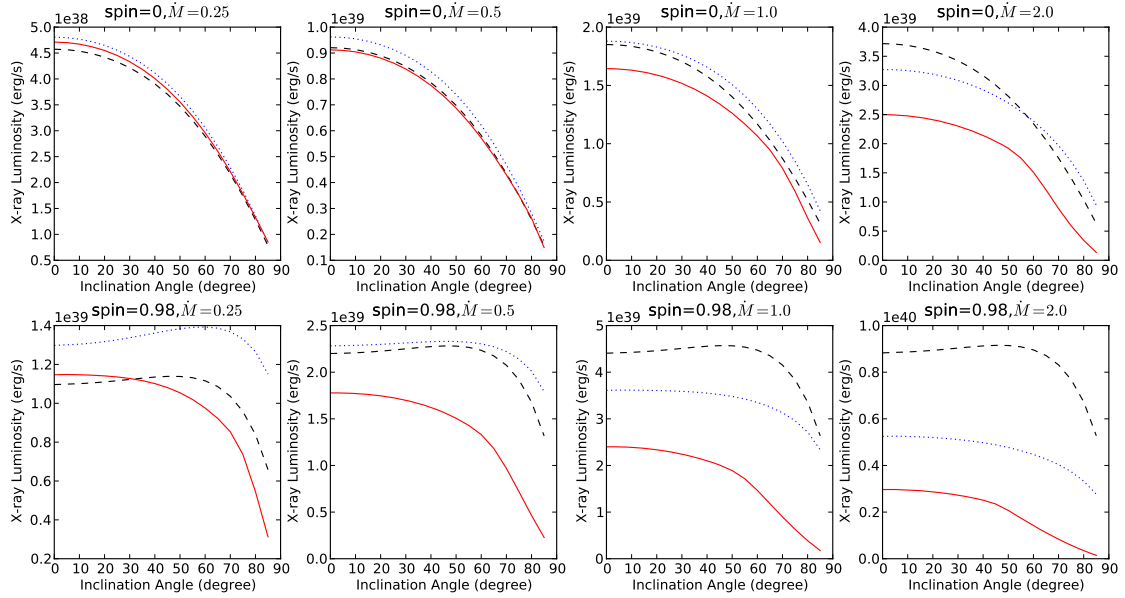


FIG. 7.— The angular dependence of the observed X-ray luminosity. As in Figure 6, the (black) dashed lines stand for the relativistic standard accretion disk, the (blue) dotted line stands for the dynamical thin accretion disk, and the (red) solid lines stand for the dynamical thick accretion disk. Different panels correspond to different black hole spin and accretion rate. The black hole mass is taken to be $10M_{\odot}$.

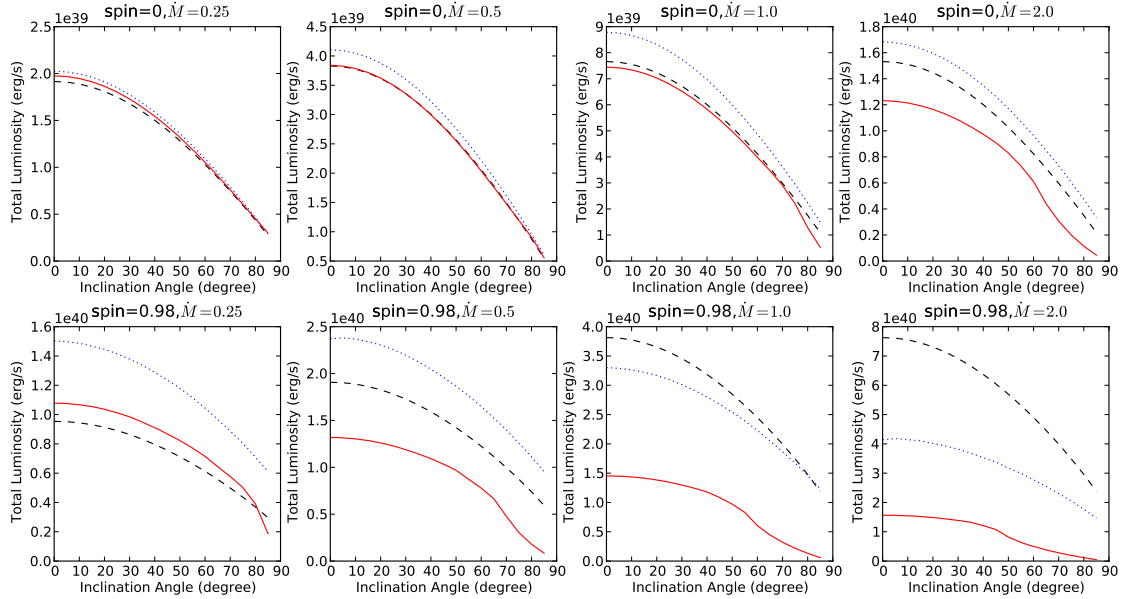


FIG. 8.— The angular dependence of the observed total luminosity. The symbol of the lines are the same as in Figure 7.

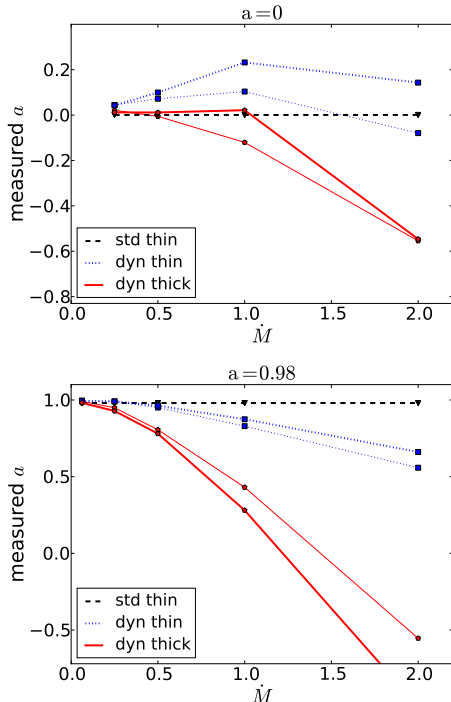


FIG. 9.— Measured spin for different models. The upper panel shows the result for a non-spinning black hole with $a = 0$, and the lower panel shows the result for a spinning black hole with $a = 0.98$. The dashed lines correspond to the thin Keplerian case (case A), the dotted lines correspond to the slim accretion disks with no thickness (case B), and the solid lines correspond to slim accretion disks with thickness effect (case C). Different line thickness represent different viewing angles: Thin lines for $\theta = 30^\circ$, and thick lines for $\theta = 60^\circ$.

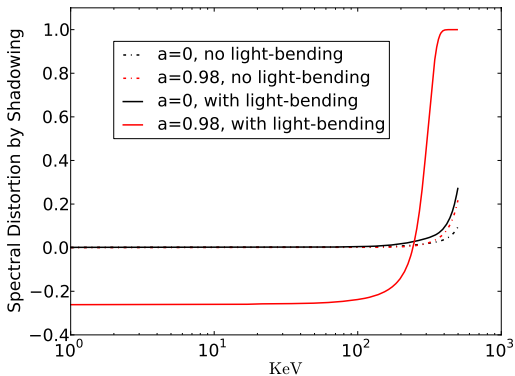


FIG. 10.— Spectral distortion (defined by Equation 30) as a function of the photon energy. The solid lines stand for the results with the effect of the light bending, while the dotted lines for the results without the light-bending effect. The red lines stand for the Kerr black hole with $a = 0.98$, and the black lines for the black hole with $a = 0$. In all the cases, the disk luminosity is the same.

the trend found in McClintock et al. (2006). At both the low (around 1/4 of Eddington luminosity) and high (close to 1 Eddington luminosity) luminosity states, our simulated result agrees well with the result of McClintock et al. (2006). When the disk luminosity is low enough, according to the spectral model we have developed, the spin determination by McClintock et al. (2006) is reliable. When the luminosity is high enough, the disk shadowing makes the measured spin lower than the actual value. This luminosity dependence of

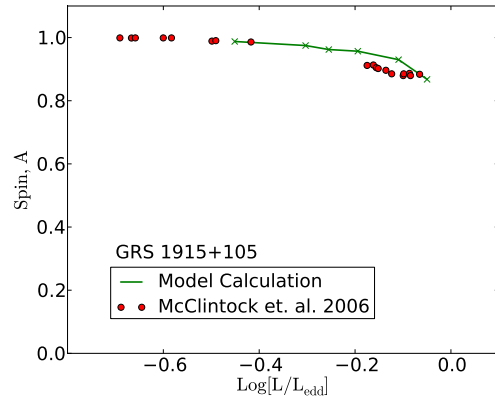


FIG. 11.— Measured spin of GRS 1915+105 as a function of the disk luminosity. The green line and dots are the results calculated in our model, including the effects of the heat advection and the disk self-shadowing. The red dots are the spin obtained in McClintock et al. (2006) by fitting the observed SED.

the measured spin is shown up both in our calculation and in the observational data. When the disk luminosity is medium (around $10^{-0.2}$ Eddington luminosity), our results begin to diverge from the data. This may due to the photon scattering by the wind from the accretion disk as suggested by Done & Davis (2008). However, as our spectra fitting is based on the model of McClintock et al. (2006), so it is still possible that different spectral model (e.g. a low temperature component, Middleton et al. 2006) may lead to a different result.

8. CONCLUSIONS

In this work, we study the structure of the relativistic slim accretion disks and their emergent spectra. Besides the effect of the photon trapping, we find that when the accretion rate is appropriate, the energy trapped in the outer regions of the accretion disks can be re-radiated in the inner regions of the accretion disks. Another main result of this work is that we check the validity of the relativistic SSD. We find that at low accretion rate, such as $\dot{M} \sim 1/4$ for $a = 0$ and $\dot{M} \sim 1/16$ for $a = 0.98$, the relativistic SSD is still valid to describe the disk structure, and the effect of heat advection will not significantly influence the global structure of the disk. At relatively high accretion rate such as $\dot{M} = 2\dot{M}_{\text{edd}}$, these effects will significantly distort the emergent spectrum, and hence affect the measurement of the black hole spin. We also find that when the accretion rate is high, the effect of the disk self-shadowing plays an even more important role than that of the heat advection alone.

The emergent luminosity from the accretion disks is angular dependent, and the degree of anisotropy is dependent on the accretion rate. In this work, we investigate the angular dependence of the observed luminosity. Due to the physical similarities between the accretion disks of different black hole mass, our result can be applied to estimate the radiation anisotropy of AGNs.

To check in principle the effect differences of spectra on estimation of spin, we create “fake” data sets with the simulated data, and fit them with the KERRBB model using XSPEC. At the relatively low accretion rate, our fitting results suggest that the simple Keplerian model is reliable. At the relatively high accretion rate, our fitting results suggest that self-shadowing effect will lead to significant under-estimation of the black

hole spin. By making our calculation relevant to the case of GRS 1915+105, without introducing additional parameters, we are able to reproduce the decrease of measured spin with the increasing luminosity, which is found in McClintock et al. (2006). This finding suggests that disk self-shadowing significantly shapes the spectra of GRS 1915+105.

There are several effects which we do not include in our calculations. It was claimed that the disk may have no time to relax to the thermodynamic equilibrium (Ohsuga et al. 2002), this effect will make our estimation of emergent flux (Equation (15)) invalid and make the disk thickness estimation inaccurate. In our calculations of the disk SED, we use a simplified model of the local spectrum and neglect the effect of limb-darkening and returning irradiation. Assuming a constant color correction may make our calculated spectra inadequate to be compared to the observation (Done & Davis 2008), so we focus on analyzing the physical effects we have introduced. The limb-darkening effect will influence the spectra and the angular dependence of the emergent luminosity,

while the returning irradiation will have some effects on both the disk structure and the emergent spectra. As Li et al. (2005) have calculated, these two effects will contribute several percents to the final results. Despite of these shortcomings, our results and the trend of the spectral evolution are still robust when the inclination angle is not too large.

We thank the anonymous referee for her/his constructive suggestions which are very helpful for the improvement of this paper and thank Prof. Jian-min Wang and Mr. Yanrong Li for discussions. G.-X. Li thanks Prof. Chris Done for discussion, and Mr. Teng Liu for help with the XSPEC software. This work is partially supported by National Basic Research Program of China (grant 2009CB824800), the National Natural Science Foundation (grants 10733010, 10673010, 10573016, 10773020, 10821302 and 10833002), the CAS (grant KJCX2-YWT03) and the Science and Technology Commission of Shanghai Municipality (10XD1405000).

REFERENCES

- Abramowicz, M. A., Chen, X.-M., Granath, M., & Lasota, J.-P. 1996, *ApJ*, 471, 762
- Abramowicz, M. A., Czerny, B., Lasota, J. P., & Szuszkiewicz, E. 1988, *ApJ*, 332, 646
- Arnaud, K. A. 1996, in *Astronomical Society of the Pacific Conference Series*, Vol. 101, *Astronomical Data Analysis Software and Systems V*, ed. G. H. Jacoby & J. Barnes, 17–+
- Begelman, M. C. 1978, *MNRAS*, 184, 53
- Begelman, M. C., & Meier, D. L. 1982, *ApJ*, 253, 873
- Beloborodov, A. M. 1998, *MNRAS*, 297, 739
- Cadez, A., Fanton, C., & Calvani, M. 1998, *New Astronomy*, 3, 647
- Carter, B. 1968, *Physical Review*, 174, 1559
- Chandrasekhar, S. 1983, *The mathematical theory of black holes*, ed. S. Chandrasekhar
- Chen, L.-H., & Wang, J.-M. 2004, *ApJ*, 614, 101
- Chen, X., & Taam, R. E. 1993, *ApJ*, 412, 254
- Cunningham, J. M., & Bardeen, C. T. 1973, *ApJ*, 183, 237
- Davis, S. W., Blaes, O. M., Hubeny, I., & Turner, N. J. 2005, *ApJ*, 621, 372
- Davis, S. W., Done, C., & Blaes, O. M. 2006, *ApJ*, 647, 525
- De Villiers, J., Hawley, J. F., & Krolik, J. H. 2003, *ApJ*, 599, 1238
- Done, C., & Davis, S. W. 2008, *ApJ*, 683, 389
- Done, C., Gierliński, M., & Kubota, A. 2007, *A&A Rev.*, 15, 1
- Fanton, C., Calvani, M., de Felice, F., & Cadez, A. 1997, *PASJ*, 49, 159
- Gammie, C. F., McKinney, J. C., & Tóth, G. 2003, *ApJ*, 589, 444
- Gammie, C. F., & Popham, R. 1998, *ApJ*, 498, 313
- Hawley, J. F., & Krolik, J. H. 2002, *ApJ*, 566, 164
- Heinzeller, D., Mineshige, S., & Ohsuga, K. 2006, *MNRAS*, 372, 1208
- Hirose, S., Krolik, J. H., & Stone, J. M. 2006, *ApJ*, 640, 901
- Igumenshchev, I. V., & Abramowicz, M. A. 2000, *ApJS*, 130, 463
- Kato, S., Fukue, J., & Mineshige, S., eds. 1998, *Black-hole accretion disks*
- Kubota, A., & Makishima, K. 2004, *ApJ*, 601, 428
- Li, L.-X., Zimmerman, E. R., Narayan, R., & McClintock, J. E. 2005, *ApJS*, 157, 335
- Liang, E. P. T., & Thompson, K. A. 1980, *ApJ*, 240, 271
- Manmoto, T. 2000, *ApJ*, 534, 734
- McClintock, J. E., Shafee, R., Narayan, R., Remillard, R. A., Davis, S. W., & Li, L.-X. 2006, *ApJ*, 652, 518
- Meyer, F., & Meyer-Hofmeister, E. 1994, *A&A*, 288, 175
- Middleton, M., Done, C., Gierliński, M., & Davis, S. W. 2006, *MNRAS*, 373, 1004
- Narayan, R. 1992, *ApJ*, 394, 261
- Narayan, R., Barret, D., & McClintock, J. E. 1997, *ApJ*, 482, 448
- Narayan, R., & Yi, I. 1994, *ApJ*, 428, L13
- . 1995, *ApJ*, 452, 710
- Noble, S. C., Krolik, J. H., & Hawley, J. F. 2010, *ApJ*, 711, 959
- Novikov, I. D., & Thorne, K. S. 1973, in *Black Holes (Les Astres Occlus)*, 343–450
- Ohsuga, K., Mineshige, S., Mori, M., & Umemura, M. 2002, *ApJ*, 574, 315
- Paczynski, B., & Bisnovatyi-Kogan, G. 1981, *Acta Astronomica*, 31, 283
- Peitz, J., & Appl. S. 1997, *MNRAS*, 286, 681
- Penna, R. F., McKinney, J. C., Narayan, R., Tchekhovskoy, A., Shafee, R., & McClintock, J. E. 2010, *ArXiv e-prints*
- Rauch, K. P., & Blandford, R. D. 1994, *ApJ*, 421, 46
- Reynolds, C. S., & Fabian, A. C. 2008, *ApJ*, 675, 1048
- Ross, R. R., Fabian, A. C., & Mineshige, S. 1992, *MNRAS*, 258, 189
- Sądowski, A., Abramowicz, M. A., Bursa, M., Kluźniak, W., Różańska, A., & Straub, O. 2009, *A&A*, 502, 7
- Sądowski, A. 2009, *ApJS*, 183, 171
- Shafee, R., McClintock, J. E., Narayan, R., Davis, S. W., Li, L.-X., & Remillard, R. A. 2006, *ApJ*, 636, L113
- Shakura, N. I., & Sunyaev, R. A. 1973, *A&A*, 24, 337
- Shimura, T., & Manmoto, T. 2003, *MNRAS*, 338, 1013
- Shimura, T., & Takahara, F. 1993, *ApJ*, 419, 78
- . 1995, *ApJ*, 445, 780
- Titarchuk, L. 1994, *ApJ*, 434, 570
- van Paradijs, J., & McClintock, J. E. 1995, in *X-ray binaries*, p. 58 - 125, ed. W. H. G. Lewin, J. van Paradijs, & E. P. J. van den Heuvel, 58–125
- Wang, J., Szuszkiewicz, E., Lu, F., & Zhou, Y. 1999, *ApJ*, 522, 839
- Wang, J., & Zhou, Y. 1999, *ApJ*, 516, 420
- Watarai, K.-y. 2006, *ApJ*, 648, 523
- Wu, S.-M., & Wang, T.-G. 2007, *MNRAS*, 378, 841
- Yuan, Y.-F., Cao, X., Huang, L., & Shen, Z.-Q. 2009, *ApJ*, 699, 722